ORIGINAL RESEARCH

Irradiation Accelerates Plaque Formation and Cellular Senescence in Flow-Altered Carotid Arteries of Apolipoprotein E Knock-Out Mice

Yu Yamamoto [ID], MD; Manabu Minami [ID], MD, PhD; Kazumichi Yoshida [ID], MD, PhD; Manabu Nagata [ID], MD; Takeshi Miyata, MD, PhD; Tao Yang, MD; Naoki Takayama [ID], MD; Keita Suzuki, MD; Masakazu Okawa, MD, PhD; Kiyofumi Yamada [ID], MD, PhD; Susumu Miyamoto, MD, PhD

BACKGROUND: Chronic inflammation through cellular senescence, known as the senescence-associated secretory phenotype, is a mechanism of various organ diseases, including atherosclerosis. Particularly, ionizing radiation (IR) contributes to cellular senescence by causing DNA damage. Although previous clinical studies have demonstrated that radiotherapy causes atherosclerosis as a long-term side effect, the detailed mechanism is unclear. This study was conducted to investigate the relationship between radiation-induced atherosclerosis and senescence-associated secretory phenotype in murine carotid arteries.

METHODS AND RESULTS: Partial ligation of the left carotid artery branches in 9-week-old male apolipoprotein E-deficient mice was performed to induce atherosclerosis. The mice received total body irradiation at a dose of 6 Gy using gamma rays at 2 weeks post operation. We compared the samples collected 4 weeks after IR with unirradiated control samples. The IR and control groups presented pathologically progressive lesions in 90.9% and 72.3% of mice, respectively. Plaque volume, macrophage accumulation, and phenotype switching of vascular smooth muscle cells were advanced in the IR group. Irradiated samples showed increased persistent DNA damage response (53BP1 [p53 binding protein 1]), upregulated cyclin-dependent kinase inhibitors (p16INK4a and p21), and elevated inflammatory chemokines expression (monocyte chemotactic protein-1, keratinocyte-derived chemokine, and macrophage inflammatory protein 2).

CONCLUSIONS: IR promoted plaque growth in murine carotid arteries. Our findings support the possibility that senescence-associated secretory phenotype aggravates atherogenesis in irradiated artery. This mice model might contribute to mechanism elucidation of radiation-induced atherosclerosis.

Key Words: atherosclerosis ■ carotid artery stenosis ■ cellular senescence ■ DNA damage ■ irradiation

R adiation-induced atherosclerosis is a long-term complication of radiotherapy. Although recent advances in cancer therapy have improved the prognosis of cancer, cardiovascular disease remains a fatal problem for people who have recovered from cancer.[1,2] Because radiotherapy for head and neck cancer elevates the risk of cerebrovascular events,[3,4] prevention

of ischemic stroke caused by radiation-induced carotid artery stenosis (RI-CS) is crucial.[5] However, the pathophysiological mechanism of radiation-induced atherosclerosis is unclear.

Recently, cellular senescence has attracted attention as a new mechanism of chronic inflammation and organ disease.[6] It has been recognized as

CLINICAL PERSPECTIVE

What Is New?
- This study provides a novel animal model of radiation-induced carotid artery stenosis and suggests that the senescence-associated secretory phenotype partially affects plaque progression.

What Are the Clinical Implications?
- This study may contribute to explication of the mechanism about radiation-induced atherosclerosis.

Nonstandard Abbreviations and Acronyms

CA	carotid artery
IR	ionizing radiation
PDDF	persistent DNA damage foci
RI-CS	radiation-induced carotid artery stenosis
SASP	senescence-associated secretory phenotype
TBI	total body irradiation
VSMC	vascular smooth muscle cell

an irreversible state of arresting cell proliferation and contributor to aging and tumor suppression. In the past few decades, the phenomenon of senescence-associated secretory phenotype (SASP) has been established as another aspect of cellular senescence, in which senescent cells with DNA damage secrete inflammatory cytokines and cause chronic inflammation in surrounding cells.[7,8] As ionizing radiation (IR) is a strong inducer of DNA damage, the possibility of SASP was also demonstrated in IR-related chronic diseases in vivo.[9]

Although DNA damage and senescent cells accumulate in atherosclerotic plaques,[10,11] how IR affects cell senescence and plaque formation is unclear. One reason for this is that no effective animal model of RI-CS has been reported. Therefore, a new protocol for developing animals that present RI-CS with a high probability is needed. Because partial ligation of the carotid artery (CA) branches was demonstrated as an experimental method for inducing atherosclerotic lesions,[12] we hypothesized that total body irradiation (TBI) under this surgical intervention would be an efficient protocol for inducing RI-CS. Moreover, we examined whether the SASP is associated with radiation-induced atherosclerosis.

METHODS

Supporting data are available from the corresponding author upon a reasonable request.

Experimental Procedures

Apolipoprotein E-deficient (ApoE$^{-/-}$) mice on a CB57BL/6J background (The Jackson Laboratory, Bar Harbor, ME) were used in all experiments. Mice were fed a western diet (F2WTD, Oriental Yeast, Tokyo, Japan) from 7 weeks old to euthanization. At 9 weeks of age, partial ligation of left CA was performed to induce an atherosclerotic lesion as previously described.[12] Briefly, the left common carotid artery was exposed under a ventral midline incision in the neck, and 3 of the 4 caudal branches (external carotid artery, internal carotid artery, and occipital artery) were ligated with an 8-0 nylon suture under a microscope so that the superior thyroid artery was left intact as an outlet for blood flow (Figure 1A). During the operation, anesthesia was intraperitoneally administered with mixed components (0.75 mg/kg dexmedetomidine; Nippon Zenyaku Kogyo, Fukushima, Japan; 4 mg/kg midazolam; Astellas Pharma, Tokyo, Japan; 5 mg/kg butorphanol; Meiji Seika Pharma, Tokyo, Japan). After the operation, the mice were recovered on a heating pad. We defined baseline as 2 weeks after partial ligation. At baseline, the mice were assigned to the IR or control groups. Mice in the IR group were treated by TBI with gamma rays from a cesium-137 source (Gammacell 40; Nordion, Otawa, Ontario, Canada) at a dose of 6 Gy. At 4 weeks after TBI, tissue samples were collected under anesthesia by intraperitoneal injection of mixed components (0.75 mg/kg dexmedetomidine;
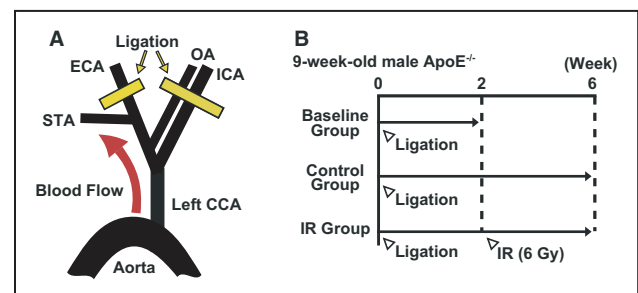
Figure 1. Experimental procedures.
A, Schematic representation of the surgical procedures. Branches of left common carotid artery (CCA) were ligated except for the superior thyroid artery (STA). STA remained intact as an outlet for blood flow. ECA indicates external carotid artery; ICA, internal carotid artery; and OA, occipital artery. **B**, Schedule of the experiments. Apolipoprotein E-deficient (ApoE$^{-/-}$) mice underwent partial ligation of the left carotid artery at 9 weeks old. At 2 weeks after ligation, mice in the baseline group were sacrificed, and mice in the ionizing radiation (IR) group was subjected to total body irradiation of 6 Gy. The IR group and control group were sacrificed at 6 weeks (4 weeks after irradiation).

Nippon Zenyaku Kogyo, Fukushima, Japan; 4 mg/kg midazolam; Astellas Pharma, Tokyo, Japan; 5 mg/kg butorphanol; Meiji Seika Pharma, Tokyo, Japan) (Figure 1B). For paraffin-embedded blocks, the CA, esophagus, trachea, and sternomastoid muscle were removed en bloc and fixed in 4% paraformaldehyde phosphate buffer. In contrast, only CAs were excised and frozen at −80°C for RNA extraction. Blood samples were collected by cardiac aspiration, and blood serum was analyzed by Oriental Yeast. Because estrogen is a modulator of atherosclerosis, only male mice were used to avoid the effects of estrogen. Animal experiments were performed in accordance with the guidelines established by Japan's Act on Welfare and Management of Animals. All procedures were approved by the Institutional Animal Care and Use Committee and Ethics Committee of Kyoto University.

Morphologic Evaluation

Samples were sliced into 5-μm thick sections with a cryostat. Sections from the portion with the most advanced atherosclerotic lesion between the bifurcation of the CA and 4 mm below the bifurcation were selected for analysis. To analyze the lesions, the sections were stained by the modified Elastica van Gieson method and observed under a bright field microscope (BZ8100; Keyence, Osaka, Japan). The intimal and medial areas of the CAs were measured using a BZ-II analyzer (Keyence). Each lesion was pathologically classified according to the modified American Heart Association criteria.[13]

Immunofluorescence and Immunohistochemistry Staining

To examine the features of the lesions between the 2 groups, samples with plaques were included. After deparaffinization and rehydration, the sections were exposed to heat-induced epitope retrieval in citrate buffer (pH 6.0). For immunofluorescence analysis, the sections were incubated with primary antibodies after blocking with 2% bovine serum albumin for 20 minutes. The sections were incubated with Alexa Fluor 488- and 594-labeled secondary antibodies (Invitrogen, Carlsbad, CA) for 2 hours at room temperature. The slides were covered with Prolong Gold antifade reagent with 4′,6-diamidino-2-phenylindole (Invitrogen). For immunohistochemistry analysis, the sections were dipped in 0.3% H_2O_2 in methanol to block peroxidase activity. The sections were incubated with primary antibodies (diluted with 2% bovine serum albumin) for 1 hour at room temperature after blocking with 2.5% normal horse serum. Following incubation with horseradish peroxidase-conjugated secondary antibodies (ImmPRESS Horse Anti-Rabbit IgG Polymer Reagent; Vector Laboratories, Burlingame, CA) for 30 minutes, the sections were visualized using a 3,3′-diaminobenzine Peroxidase Substrate Kit (Vector Laboratories) with hematoxylin counterstaining.

The following antibodies were used: anti-alpha-smooth muscle actin (19245, rabbit monoclonal, 1:200, Cell Signaling Technology, Danvers, MA), antivimentin (Alexa Fluor 488 conjugate, 9854, rabbit monoclonal, 1:200, Cell Signaling Technology), anti-Iba-1 (013-27691, rabbit polyclonal, 1:1000, Fujifilm Wako, Osaka, Japan), anti-gamma H2AX (05-636-I, mouse monoclonal, 1:250, Millipore, Billerica, MA), anti-53BP1 (p53 binding protein 1; NB100-304, rabbit polyclonal, 1:1000 and Alexa Fluor 594 conjugate, NB100-304AF594, rabbit polyclonal, 1:100, Novus Biologicals, Littleton, CO), anti-p16INK4a (10883-1-AP, rabbit polyclonal, 1:300, Proteintech, Rosemont, IL), and anti-p21 (bs-10129R, rabbit polyclonal, 1:100, Bioss, Woburn, MA). The slides were observed under a fluorescence microscope (BZ-X710; Keyence) and images were analyzed using a BZ-X analyzer (Keyence).

Quantitative Real-Time Polymerase Chain Reaction

Total RNA was extracted from the CAs with a RNeasy Micro kit (QIAGEN, Hilden, Germany) and first-strand cDNA was generated using High-Capacity cDNA Reverse Transcription Kits (Thermo Fisher Scientific, Waltham, MA). Two left CAs were combined to obtain a sufficient amount of RNA per sample. Quantitative real-time polymerase chain reaction was performed using THUNDERBIRD SYBR qPCR Mix (TOYOBO, Osaka, Japan) and an Applied Biosystems 7300 Real-Time PCR System (Applied Biosystems, Foster City, CA). The data were analyzed using the ΔΔCT method and normalized to the expression of the β-actin gene. Primers with the following sequences were used for polymerase chain reaction: p16INK4a, 5′-CATGTTGTTGAGGCTAGAGAGG-3′ (forward) and 5′-CACCGTAGTTGAGCAGAAGAG-3′ (reverse), p21, 5′-CTAGAACAGGGATGGCAGTTAG-3′ (forward) and 5′-GAGCAGCAGATCACCAGATTA-3′ (reverse), monocyte chemotactic protein-1 (MCP-1), 5′-GAAGGAATGGGTCCAGACATAC-3′ (forward) and 5′-TCACACTGGTCACTCCTACA-3′ (reverse), keratinocyte-derived chemokine (KC), 5′-GCTGGCTTCTGACAACACTAT-3′ (forward) and 5′-TTCGCACAACACCCTTCTAC-3′ (reverse), macrophage inflammatory protein 2 (MIP-2), 5′-TAAGCACCGAGGAGAGTAGAA-3′ (forward) and 5′-GTGCCTTACGAGGAAGACATAA-3′ (reverse), β-actin, 5′-TGTGACGTTGACATCCGTAAA-3′ (forward) and 5′-TAGGAGCCAGAGCAGTAATCT-3′ (reverse).

Statistical Analysis

All data are presented as the mean and SD. Data were statistically analyzed using the Mann–Whitney U test with GraphPad Prism version 8 software (GraphPad, Inc., San Diego, CA). A $P<0.05$ was considered to indicate statistical significance.

RESULTS

Effects of TBI on Body Weight and Serum Lipid Profile

A total of 74 mice was used in this study. Three of 34 mice (8.82%) assigned to the IR group died after TBI. Mice in the IR group showed a reduced body weight at 2 weeks after irradiation, which recovered by 4 weeks. Mice in the control group showed a gradual increase in body weight and significantly higher increase ratio than those in the IR group (IR group: 2.96±6.47%; control group: 15.5±4.80%; n=11 each, $P<0.001$; Figure 2A). The 2 groups showed no significant differences in serum lipid parameters: total cholesterol, triglyceride, nonesterified fatty acid, low-density lipoprotein cholesterol, and high-density lipoprotein cholesterol. Serum albumin level showed no significant differences between the 2 groups, but total protein
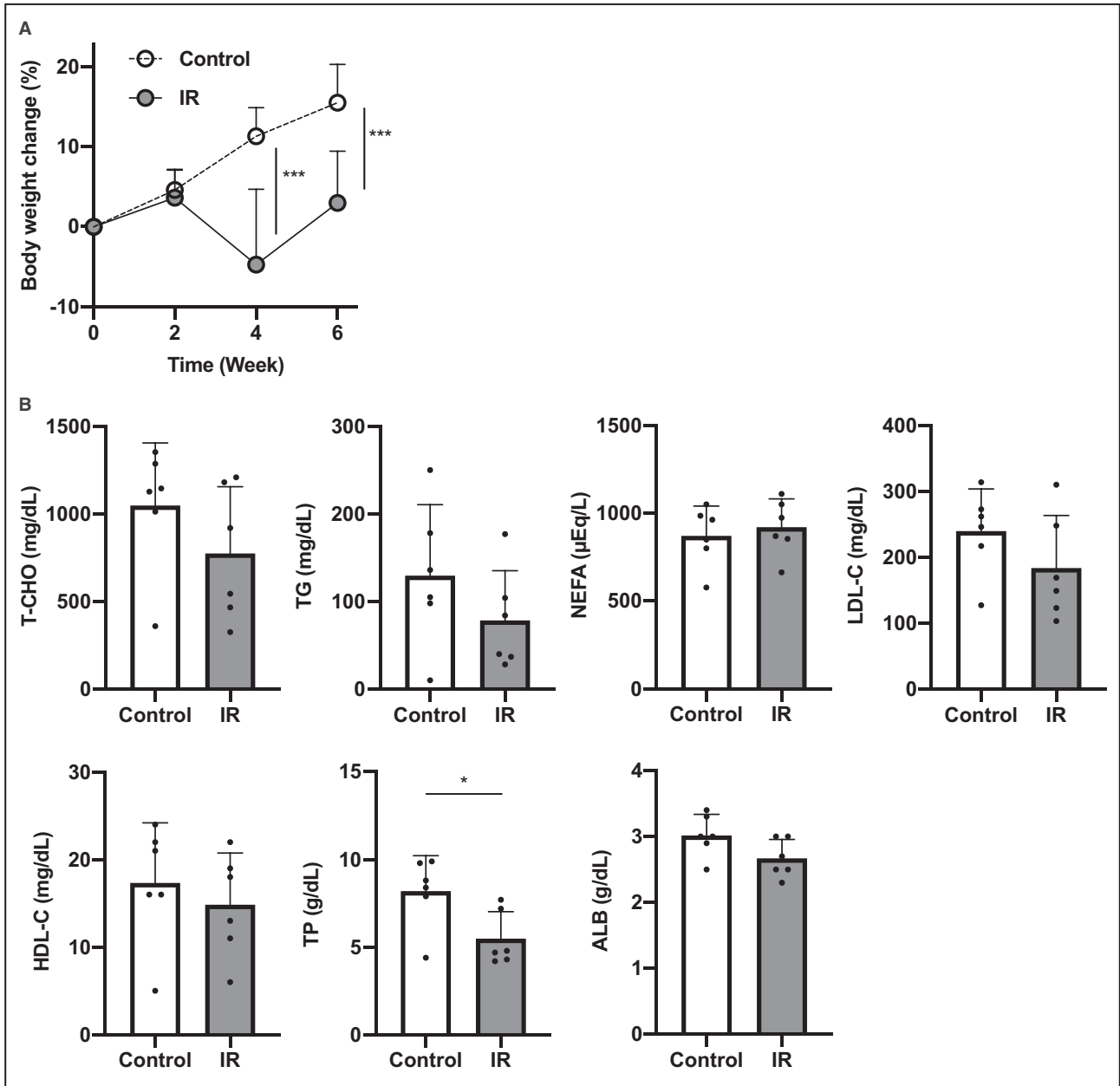
Figure 2.   General health.
A, Body weight change (n=11 each). Irradiated mice presented lower increase in body weight after ionizing radiation (IR) than control. **B**, Blood test results (n=6 each). Serum lipid profile and albumin (ALB) level showed no significant differences between the 2 groups. The IR group presented significant lower total protein (TP) level than the control group. Data are expressed as the mean±SD for each group. (HDL-C indicates high-density lipoprotein cholesterol; LDL-C, low-density lipoprotein cholesterol; NEFA, non-esterified fatty acid; T-CHO, total cholesterol; and TG, triglyceride). *$P<0.05$ or ***$P<0.001$ vs the control group, as determined by Mann-Whitney U test.

level was significantly lower in the IR group than in the control group (IR group: 5.48±1.55 g/dL, control group: 8.20±2.02 g/dL, n=6 each, $P<0.05$; Figure 2B).

IR Induces Plaque Progression

Pathologically progressive lesions were observed in 25.0% (2 of 8 mice) in the baseline group, 72.7% (8 of 11 mice) in the control group, and 90.9% (10 of 11 mice) in the IR group (Figure 3A and 3B). The intimal area was significantly larger in the IR group than in the control group (IR group: $7.52±3.75×10^4$ μm^2; control group: $4.07±2.51×10^4$ μm^2, n=11 each; $P<0.05$; Figure 3C). The intima media ratio was also elevated by IR (IR group: 1.68±0.850; control group: 0.855±0.514, n=11 each; $P<0.05$; Figure 3C).

IR Promotes Macrophage Accumulation and Phenotype Switching of Vascular Smooth Muscle Cells in Plaques

To evaluate plaque features, we investigated macrophage accumulation and phenotype switching in vascular smooth muscle cells (VSMCs). Iba-1 (ionized calcium-binding adaptor protein-1) was used to identify macrophages.[14] Plaques in the IR group contained Iba-1-positive cells at a higher rate than those in the control group (IR group: 12.9±4.78%; control group: 7.99±3.70%, n=6 each; $P<0.05$; Figure 4A and 4B). The contractile phenotype and synthetic phenotype of VSMCs were examined by detecting alpha-smooth muscle actin and vimentin, respectively.[15] We observed low expression of alpha-smooth muscle actin and high expression of vimentin in the plaques of IR group (Figure 4C). Vimentin to alpha-smooth muscle actin area ratio in the intima was significantly higher in the IR group than in the control group (IR group: 0.941±0.162; control group: 0.402±0.113, n=5 each; $P<0.01$; Figure 4D).

IR Promotes Persistent DNA Damage in Plaque

To investigate whether TBI at a dose of 6 Gy is sufficient to induce DNA damage in the CAs, we evaluated the expression of DNA damage markers in samples collected immediately after IR. Gamma H2AX and 53BP1 were used to detect DNA double-strand breaks.[16,17] Immunofluorescence staining
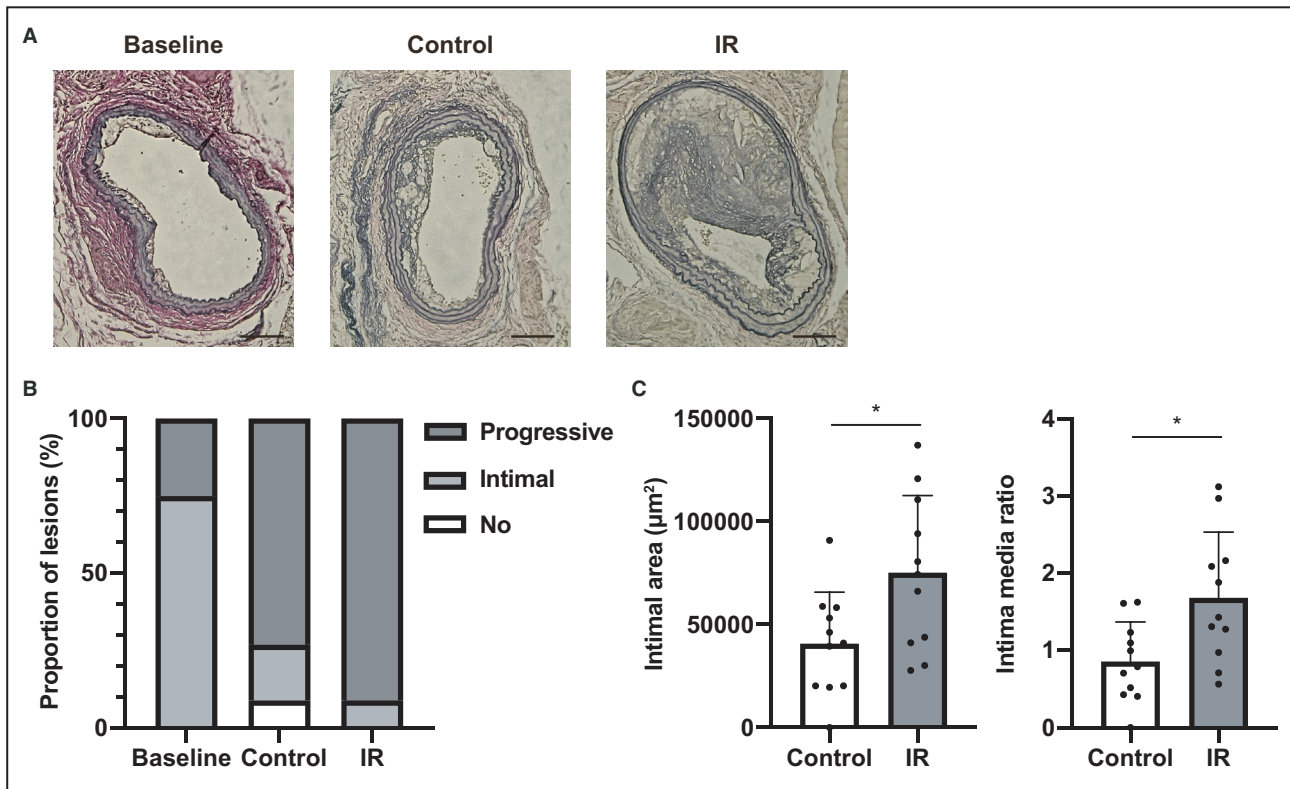

Figure 3. Ionizing radiation (IR) accelerated atherosclerosis in carotid arteries (CAs).
A, Representative images of CAs stained by modified Elastica van Gieson staining. Scale bar indicates 100 µm. **B**, Pathological classification of the lesions according to the modified American Heart Association criteria (n=8 in the baseline group, n=11 each in the control and IR groups). **C**, Morphological measurements of intimal area and intima media ratio (n=11 each). Data are expressed as the mean±SD for each group. *$P<0.05$ vs the control group, as determined by Mann-Whitney U test.
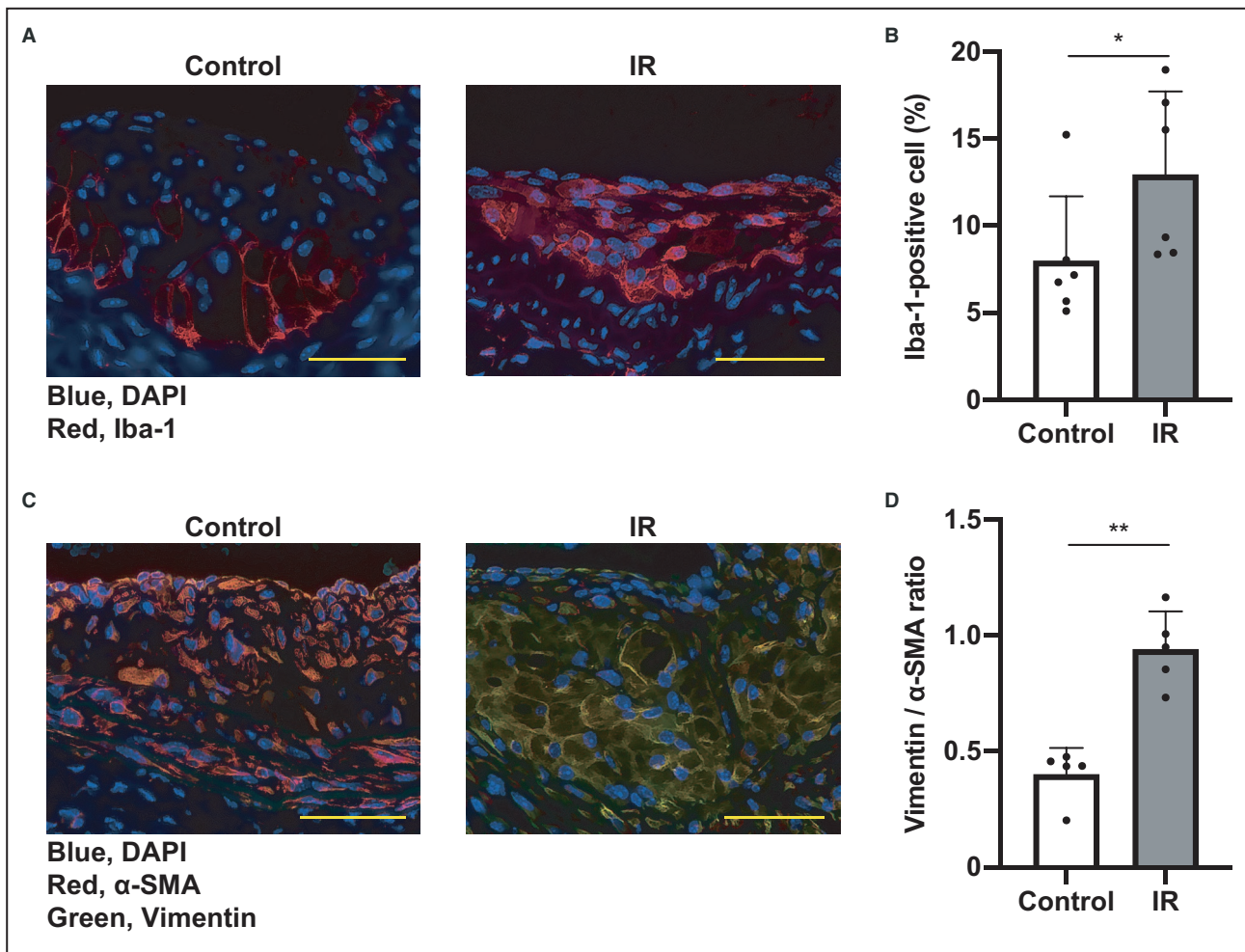
Figure 4.   Increased accumulation of macrophages and advanced switching of the vascular smooth muscle cell phenotype in irradiated carotid arteries.

A, Representative image of immunofluorescence staining for Iba-1 (red) in carotid arteries. Iba-1 was highly expressed in irradiated plaque compared with in the control. **B**, Percentage of Iba-1-positive cells in the intima between the IR and control groups (n=6 each). **C**, Representative image of multicolor staining with vimentin (green) and alpha-smooth muscle actin (α-SMA, red). The irradiated plaques showed higher expression of vimentin and lower expression of α-SMA than control. **D**, Vimentin to α-SMA area ratio in the intima (n=5 each). Scale bar indicates 50 μm. Data are expressed as the mean±SD for each group. *$P<0.05$ or **$P<0.01$ vs the control group, as determined by Mann-Whitney U test. DAPI indicates 4′,6-diamidino-2-phenylindole; Iba-1, ionized calcium-binding adaptor protein-1; and IR, ionizing radiation.

revealed broad expression of gamma H2AX and 53BP1 foci in samples collected at 2 hours after irradiation (Figure 5A), whereas expression of these markers was not observed in unirradiated samples (data not shown). Persistent DNA damage was observed as the expression of 53BP1 foci. 53BP foci remained in the intima and media at 4 weeks after irradiation. The proportion of 53BP1-positive cells in the IR group was significantly elevated compared with that in the control group in both intima (IR group: 3.10±0.911%; control group: 0.481±0.437%, n=7 each; $P<0.001$) and media (IR group: 2.52±1.85%; control group: 0.403±0.394%, n=7 each; $P<0.05$) (Figure 5B).

To investigate the features of 53BP1-positive cells in plaques, we examined the localization of 53BP1 by multicolor immunofluorescence staining. Most 53BP1-positive cells in irradiated plaques were also vimentin positive (81.3±7.55%, n=6; Figure 5C and 5E). In contrast, 53BP1 and Iba-1 showed relatively low colocalization (9.96±6.13%, n=6; Figure 5D and 5E).

Senescence Is Promoted in CA Plaques by IR

Next, we investigated the expression of cyclin-dependent kinase inhibitor proteins (p16INK4a and p21) to evaluate cellular senescence. Cyclin-dependent
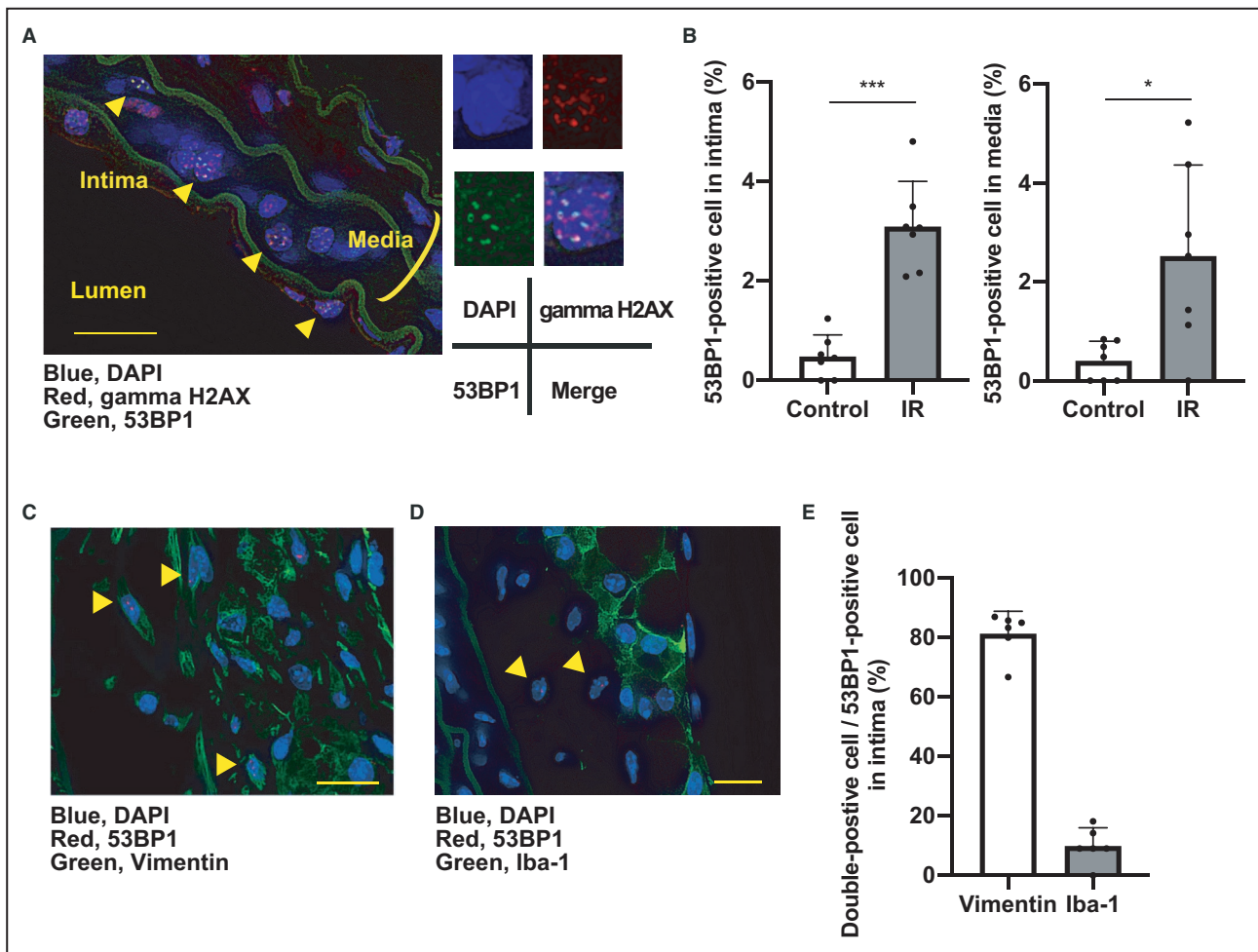
Figure 5. Irradiated carotid arteries (CAs) presented DNA damage after radiation exposure.
A, Representative image of multiple immunofluorescence staining with gamma H2AX (red), 53BP1 (green), and 4′, 6-diamidino-2-phenylindole (DAPI, blue) using samples collected at 2 hours after ionizing radiation (IR). Expression of DNA damage markers, gamma H2AX and 53BP1, was broadly observed in both the intima and media of the CA. **B**, Proportion of 53BP1-positive cells in the intima (left) and media (right) at 4 weeks after IR. Expression of 53BP1 foci in the IR group was significantly higher than in the control group (n=7 each). **C** and **D**, Representative images of multicolor immunofluorescence staining using samples from the IR group. 53BP1 foci (red) were expressed in vimentin-positive cells (green) (**C**). In contrast, Iba-1 (green) was expressed separately from the 53BP1 foci (red) (**D**). **E**, Ratio of vimentin/Iba-1-positive cells in the intimal area among cells with 53BP1 foci (n=6 each). Scale bar indicates 20 µm. Data are presented as the mean±SD. *$P<0.05$ or ***$P<0.001$ vs the control group (Mann-Whitney U test). 53BP1 indicates p53 binding protein 1; DAPI indicates 4′,6-diamidino-2-phenylindole; and Iba-1, ionized calcium-binding adaptor protein-1; and H2AX, histon e 5 protein 2ax.

kinase inhibitors promote cell cycle arrest, and the up-regulation of p16INK4a and p21 is a characteristic of cellular senescence.[18,19] Irradiated plaques contained p16INK4a- and p21-positive cells at a higher rate than those in unirradiated plaques (Figure 6A and 6C). Intimal cells positively stained for p16INK4a and p21 were significantly higher in the IR group than in the control group (p16INK4a, IR group: 75.0±6.52%; control group: 55.7±6.43%, n=6–7; $P<0.01$, p21, IR group: 89.8±3.62%; control group: 73.5±3.83%, n=6 each; $P<0.01$; Figure 6B and 6D). Similarly, mRNA expression levels of p16INK4a and p21 were significantly higher in the IR group than in the control group (p16INK4a, IR group: 1.75±0.765; control group: 1.00±0.281, n=9–10;

$P<0.05$, p21, IR group: 1.67±0.678; control group: 1.00±0.367, n=7 each; $P<0.05$; Figure 6E).

Influence of IR on Inflammatory Gene Expression

We performed quantitative real-time polymerase chain reaction to investigate whether IR induced the expression of inflammatory genes in CAs. Compared with the control group, mRNA expression levels of MCP-1, KC, and MIP-2 were significantly higher in the IR group (MCP-1, IR group: 1.71±0.760; control group: 1.00±0.374, n=9–10; $P<0.05$, KC, IR group: 4.63±5.53; control group: 1.00±0.797, n=9–10; $P<0.05$, MIP-2, IR
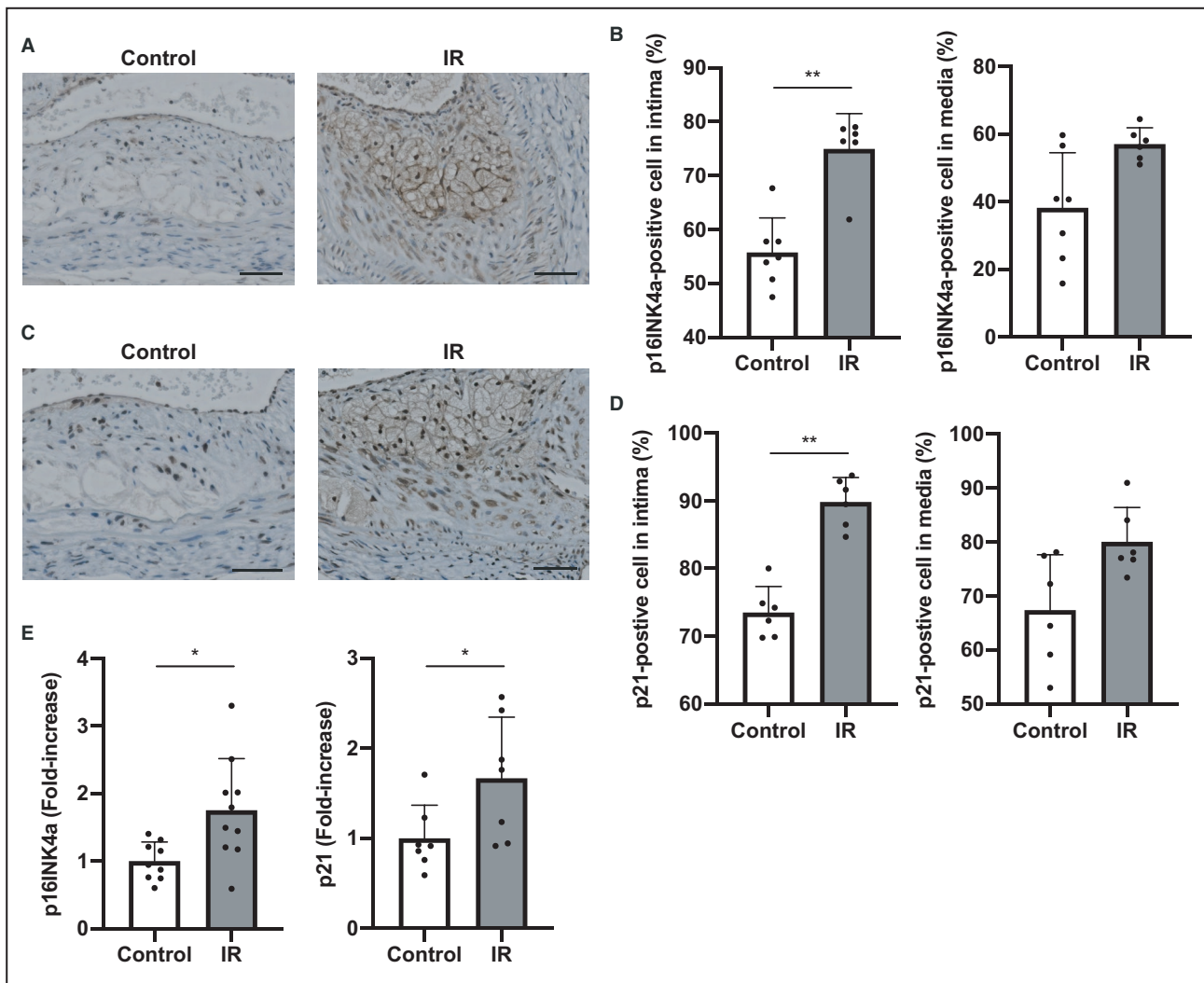
Figure 6. Cellular senescence advanced in irradiated carotid arteries (CAs).
Representative images of immunohistochemistry for p16INK4a (**A**) and p21 (**C**). Scale bar indicates 20 μm. Expression of both markers was significantly higher in the intima of the IR group than in the control group (**B**, p16INK4a; **D**, p21, n=6–7 per group). **E**, mRNA expression levels of p16INK4a (left) and p21 (right) were increased by IR (n=7–10 per group). Data are presented as the mean±SD. *P<0.05, **P<0.01 vs the control group, as determined by Mann-Whitney U test. IR indicates ionizing radiation.

group: 4.63±3.57; control group: 1.00±0.899, n=9–10; P<0.01, Figure 7).

DISCUSSION

In this study, irradiated murine CAs with altered blood flow showed plaque progression accompanied by increased persistent DNA damage, cellular senescence, and inflammatory gene expression. These results support that SASP partially affects the development of RI-CS.

Previous in vivo studies of RI-CS have revealed the atherogenesis of RI and the difficulty of obtaining advanced plaques in murine CAs, even after long-term observation.[20,21] By performing partial ligation of CAs, this protocol resulted in IR-accelerated plaque

formation. Plaque progression is supported by both increased plaque volume, advanced switching of the VSMC phenotype, and increased accumulation of macrophages. This protocol was effective for generating CA plaques because of the higher probability of plaque formation and shorter experimental period. In addition, more than half of mice in the control group presented progressive lesions, enabling examination of plaque features with or without IR. Because all organs were irradiated in this protocol, the lower body weight increase and lower serum total protein level in the IR group were thought to result from appetite loss and gastrointestinal symptoms, known as acute radiation syndrome.[22,23] TBI at a dose of >6 Gy causes an increase in mortality.[24] Therefore, irradiation using TBI at a dose of 6 Gy is a tolerable fatality rate. However, the
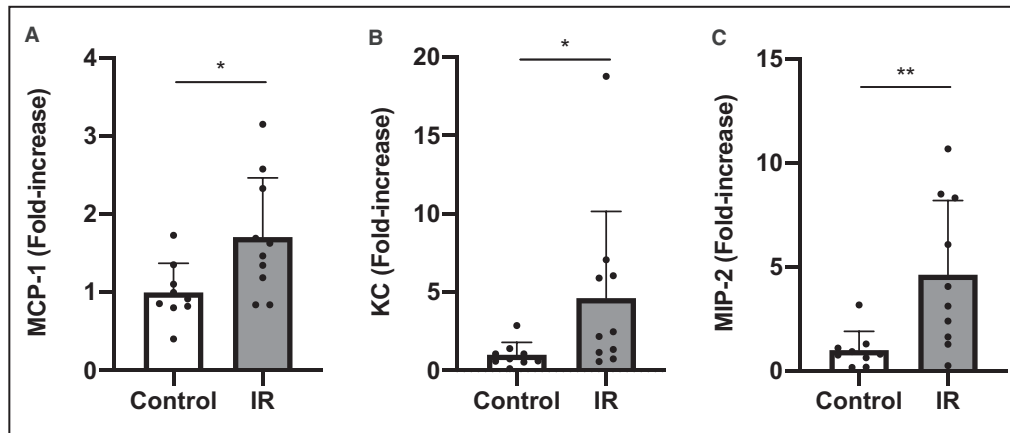
Figure 7. mRNA expression levels of inflammatory chemokines in carotid arteries (CAs).
A, Monocyte chemotactic protein-1 (MCP-1), (**B**) keratinocyte-derived chemokine (KC), and (**C**) macrophage inflammatory protein 2 (MIP-2). Irradiated CAs presented significantly higher expression of each factor than control (n=9–10 each group). Data are expressed as the mean±SD. IR indicates ionizing radiation. *$P<0.05$ or **$P<0.01$ vs the control group (Mann-Whitney U test).

local irradiation at a much higher dose is often employed in the radiotherapy to treat cancers. Hence, the effects of irradiation may not be directly applicable in a clinical setting.

DNA damage is a fundamental mechanism by which radiation causes cellular damage. As soon as DNA damage occurs because of cytotoxic effects, the DNA repair pathway and DNA damage response are activated. Double-strand breaks are the most crucial type of DNA damage. Although most double-strand breaks are transient and quickly repaired, some remain irreparable. Persistent DNA damage foci (PDDF) after IR have been observed both in vitro and in vivo.[7,25] In the current study, irradiated CAs contained PDDF more frequently than unirradiated CAs, indicating the existence of a persistent DNA damage response in irradiated plaques. Further, most cells with PDDF in CA plaques were also vimentin positive. This result indicates that the irreparable DNA damage response was sustained mainly in dedifferentiated VSMCs. Two hypotheses were proposed: undifferentiated VSMCs that had already existed in the intima at IR presented with PDDF, or damaged VSMCs in the media migrated to the intima after irradiation. The latter hypothesis is supported by a previous study in which gamma irradiation changed VSMCs to a dedifferentiated phenotype and promoted VSMC migration.[26] PDDF in VSMCs indicated that local DNA damage was sustained in irradiated CAs because most VSMCs in plaques are derived from local VSMCs rather than from hematopoietic cells.[27,28]

Because persistent DNA damage response causes cellular senescence,[7] PDDF may contributes to the promotion of cellular senescence in this irradiated plaque model. However, a discrepancy was observed between the extents of persistent DNA damage and cellular senescence; the difference in senescent marker expression between the IR group and control group was much higher than the difference in 53BP1 expression between these groups. This may be because of the paracrine effect of SASP, indicating that senescent cells with PDDF secrete inflammasomes and cause surrounding cells to become senescent.[29,30]

Based on the high frequency of p16INK4a- or p21-positive cells observed in the irradiated plaques, most irradiated VSMCs in the plaques demonstrated the characteristic features of cellular senescence. Senescent VSMCs secrete inflammatory cytokines such as chemokines,[31,32] showing aspects of SASP. Collectively, our results support that IR promotes inflammation and plaque progression through SASP in murine CAs, at least reflecting local DNA damage. In addition, the senescence of VSMCs decreases collagen and extracellular matrix secretion[32] and pathologically causes plaque vulnerability by promoting the necrotic core and reducing the fibrin cap.[33] A clinical report showed that human radiation-induced plaque obtained from carotid endarterectomy presented vulnerability with intraplaque hemorrhage and a necrotic core.[34] Such features were not evaluated in this study. Further studies are needed to determine how senescent cells affect plaque instability.

The present study had 2 limitations. First, the present study presented the possibility of SASP in RI-CS but did not present the precise evaluation of SASP. In future research, inhibitory tests for examination of the senescence pathway are essential, and various mechanisms other than SASP should be evaluated. Especially, apoptosis due to DNA damage, which also promotes atherosclerosis, may coexist with SASP in this mouse model.

Furthermore, cellular senescence should be evaluated in a multidirectional manner, including senescence-associated beta-galactosidase. Second, this protocol involved causing not only local DNA damage but also systemic DNA damage through whole-body exposure of radiation. Therefore, local and systemic effects cannot be delineated. For example, we cannot confirm whether Iba-1-positive cells with 53BP1 foci indicate newly invasive macrophages after IR or preexisting macrophages at IR. Because hematopoietic stem cell senescence induced by TBI has been demonstrated in vivo,[35] SASP in irradiated plaques might partly result from bone marrow damage. Clonal hematopoiesis intermediate potential, a premalignant state due to clonal expansion of hematopoietic cells, was recently observed as a pattern of bone marrow damage.[36] Because clonal hematopoiesis intermediate potential has attracted attention as a new mechanism of atherosclerosis,[37,38] this mouse model may also exhibit its influence. To distinguish local effects from total body effects, further studies of local irradiation only of the neck, or TBI except for the neck, must be performed.

Analysis of our developed animal model of RI-CS suggested that radiation aggravates atherosclerosis via SASP. Therefore, our findings provide insight into the mechanism underlying IR-induced atherosclerosis.

CONCLUSIONS

This study showed that irradiation accelerated plaque formation in murine CAs with altered blood flow. The irradiated plaques exhibited a persistent DNA damage response, progression of cellular senescence, and inflammation. Based on our findings, the formation of RI-CSs can be partly explained by SASP.

Affiliations

Department of Neurosurgery (Y.Y., K. Yoshida, M.N., T.M., T.Y., N.T., K.S., M.O., K. Yamada, S.M.) and Department of Clinical Innovative Medicine (Y.Y., M.M., M.N., T.M., T.Y.), Kyoto University Graduate School of Medicine, Kyoto, Japan; and Department of Data Science, National Cerebral and Cardiovascular Center, Suita, Japan (M.M.).

REFERENCES

1. Sturgeon KM, Deng L, Bluethmann SM, Zhou S, Trifiletti DM, Jiang C, Kelly SP, Zaorsky NG. A population-based study of cardiovascular disease mortality risk in US cancer patients. *Eur Heart J*. 2019;40:3889–3897. DOI: 10.1093/eurheartj/ehz766.

2. Darby SC, Ewertz M, McGale P, Bennet AM, Blom-Goldman U, Brønnum D, Correa C, Cutter D, Gagliardi G, Gigante B, et al. Risk of ischemic heart disease in women after radiotherapy for breast cancer. *N Engl J Med*. 2013;368:987–998. DOI: 10.1056/NEJMoa1209825.

3. Scott AS, Parr LA, Johnstone PA. Risk of cerebrovascular events after neck and supraclavicular radiotherapy: a systematic review. *Radiother Oncol*. 2009;90:163–165. DOI: 10.1016/j.radonc.2008.12.019.

4. Plummer C, Henderson RD, O'Sullivan JD, Read SJ. Ischemic stroke and transient ischemic attack after head and neck radiotherapy: a review. *Stroke*. 2011;42:2410–2418. DOI: 10.1161/STROKEAHA.111.615203.

5. Liao W, Zheng Y, Bi S, Zhang B, Xiong Y, Li YI, Fang W, Xiao S, Yang L, Thea A, et al. Carotid stenosis prevalence after radiotherapy in nasopharyngeal carcinoma: a meta-analysis. *Radiother Oncol*. 2019;133:167–175. DOI: 10.1016/j.radonc.2018.11.013.

6. Childs BG, Durik M, Baker DJ, van Deursen JM. Cellular senescence in aging and age-related disease: from mechanisms to therapy. *Nat Med*. 2015;21:1424–1435. DOI: 10.1038/nm.4000.

7. Rodier F, Coppé JP, Patil CK, Hoeijmakers WA, Muñoz DP, Raza SR, Freund A, Campeau E, Davalos AR, Campisi J. Persistent DNA damage signalling triggers senescence-associated inflammatory cytokine secretion. *Nat Cell Biol*. 2009;11:973–979. DOI: 10.1038/ncb1909.

8. Rodier F, Muñoz DP, Teachenor R, Chu V, Le O, Bhaumik D, Coppé J-P, Campeau E, Beauséjour CM, Kim S-H, et al. DNA-scars: distinct nuclear structures that sustain damage-induced senescence growth arrest and inflammatory cytokine secretion. *J Cell Sci*. 2011;124:68–81. DOI: 10.1242/jcs.071340.

9. Aratani S, Tagawa M, Nagasaka S, Sakai Y, Shimizu A, Tsuruoka S. Radiation-induced premature cellular senescence involved in glomerular diseases in rats. *Sci Rep*. 2018;8:16812. DOI: 10.1038/s41598-018-34893-8.

10. Martinet W, Knaapen MW, De Meyer GR, Herman AG, Kockx MM. Elevated levels of oxidative DNA damage and DNA repair enzymes in human atherosclerotic plaques. *Circulation*. 2002;106:927–932. DOI: 10.1161/01.CIR.0000026393.47805.21.

11. Childs BG, Baker DJ, Wijshake T, Conover CA, Campisi J, van Deursen JM. Senescent intimal foam cells are deleterious at all stages of atherosclerosis. *Science*. 2016;354:472–477. DOI: 10.1126/science.aaf6659.

12. Nam D, Ni CW, Rezvan A, Suo J, Budzyn K, Llanos A, Harrison D, Giddens D, Jo H. Partial carotid ligation is a model of acutely induced disturbed flow, leading to rapid endothelial dysfunction and atherosclerosis. *Am J Physiol Heart Circ Physiol*. 2009;297:H1535–H1543. DOI: 10.1152/ajpheart.00510.2009.

13. Virmani R, Kolodgie FD, Burke AP, Farb A, Schwartz SM. Lessons from sudden coronary death: a comprehensive morphological classification scheme for atherosclerotic lesions. *Arterioscler Thromb Vasc Biol*. 2000;20:1262–1275. DOI: 10.1161/01.ATV.20.5.1262.

14. Tian Y, Kelemen SE, Autieri MV. Inhibition of AIF-1 expression by constitutive siRNA expression reduces macrophage migration, proliferation, and signal transduction initiated by atherogenic stimuli. *Am J Physiol Cell Physiol*. 2006;290:C1083–C1091. DOI: 10.1152/ajpcell.00381.2005.

15. Worth NF, Rolfe BE, Song J, Campbell GR. Vascular smooth muscle cell phenotypic modulation in culture is associated with reorganisation of contractile and cytoskeletal proteins. *Cell Motil Cytoskeleton*. 2001;49:130–145. DOI: 10.1002/cm.1027.

16. Kuo LJ, Yang LX. Gamma-H2AX—a novel biomarker for DNA double-strand breaks. *In Vivo*. 2008;22:305–309.

17. Anderson L, Henderson C, Adachi Y. Phosphorylation and rapid relocalization of 53BP1 to nuclear foci upon DNA damage. *Mol Cell Biol*. 2001;21:1719–1729. DOI: 10.1128/MCB.21.5.1719-1729.2001.

18. Alcorta DA, Xiong Y, Phelps D, Hannon G, Beach D, Barrett JC. Involvement of the cyclin-dependent kinase inhibitor p16 (INK4a) in replicative senescence of normal human fibroblasts. *Proc Natl Acad Sci USA*. 1996;93:13742–13747. DOI: 10.1073/pnas.93.24.13742.

19. Stein GH, Drullinger LF, Soulard A, Dulić V. Differential roles for cyclin-dependent kinase inhibitors p21 and p16 in the mechanisms of senescence and differentiation in human fibroblasts. *Mol Cell Biol*. 1999;19:2109–2117. DOI: 10.1128/MCB.19.3.2109.

20. Hoving S, Heeneman S, Gijbels MJ, te Poele JA, Russell NS, Daemen MJ, Stewart FA. Single-dose and fractionated irradiation promote initiation and progression of atherosclerosis and induce an inflammatory

plaque phenotype in ApoE(-/-) mice. *Int J Radiat Oncol Biol Phys.* 2008;71:848–857. DOI: 10.1016/j.ijrobp.2008.02.031.

21. Stewart FA, Heeneman S, Te Poele J, Kruse J, Russell NS, Gijbels M, Daemen M. Ionizing radiation accelerates the development of atherosclerotic lesions in ApoE-/- mice and predisposes to an inflammatory plaque phenotype prone to hemorrhage. *Am J Pathol.* 2006;168:649–658. DOI: 10.2353/ajpath.2006.050409.

22. Singh VK, Seed TM. A review of radiation countermeasures focusing on injury-specific medicinals and regulatory approval status: part I. Radiation sub-syndromes, animal models and FDA-approved countermeasures. *Int J Radiat Biol.* 2017;93:851–869. DOI: 10.1080/09553002.2017.1332438.

23. Booth C, Tudor G, Tudor J, Katz BP, MacVittie TJ. Acute gastrointestinal syndrome in high-dose irradiated mice. *Health Phys.* 2012;103:383–399. DOI: 10.1097/HP.0b013e318266ee13.

24. Koch A, Gulani J, King G, Hieber K, Chappell M, Ossetrova N. Establishment of early endpoints in mouse total-body irradiation model. *PLoS One.* 2016;11:e0161079. DOI: 10.1371/journal.pone.0161079.

25. Le ON, Rodier F, Fontaine F, Coppe JP, Campisi J, DeGregori J, Laverdière C, Kokta V, Haddad E, Beauséjour CM. Ionizing radiation-induced long-term expression of senescence markers in mice is independent of p53 and immune status. *Aging Cell.* 2010;9:398–409. DOI: 10.1111/j.1474-9726.2010.00567.x.

26. Milliat F, François A, Isoir M, Deutsch E, Tamarat R, Tarlet G, Atfi A, Validire P, Bourhis J, Sabourin J-C, et al. Influence of endothelial cells on vascular smooth muscle cells phenotype after irradiation: implication in radiation-induced vascular damages. *Am J Pathol.* 2006;169:1484–1495. DOI: 10.2353/ajpath.2006.060116.

27. Bentzon JF, Sondergaard CS, Kassem M, Falk E. Smooth muscle cells healing atherosclerotic plaque disruptions are of local, not blood, origin in apolipoprotein E knockout mice. *Circulation.* 2007;116:2053–2061. DOI: 10.1161/CIRCULATIONAHA.107.722355.

28. Daniel JM, Bielenberg W, Stieger P, Weinert S, Tillmanns H, Sedding DG. Time-course analysis on the differentiation of bone marrow-derived progenitor cells into smooth muscle cells during neointima formation. *Arterioscler Thromb Vasc Biol.* 2010;30:1890–1896. DOI: 10.1161/ATVBAHA.110.209692.

29. Nelson G, Wordsworth J, Wang C, Jurk D, Lawless C, Martin-Ruiz C, von Zglinicki T. A senescent cell bystander effect: senescence-induced senescence. *Aging Cell.* 2012;11:345–349. DOI: 10.1111/j.1474-9726.2012.00795.x.

30. Acosta JC, Banito A, Wuestefeld T, Georgilis A, Janich P, Morton JP, Athineos D, Kang T-W, Lasitschka F, Andrulis M, et al. A complex secretory program orchestrated by the inflammasome controls paracrine senescence. *Nat Cell Biol.* 2013;15:978–990. DOI: 10.1038/ncb2784.

31. Song Y, Shen H, Schenten D, Shan P, Lee PJ, Goldstein DR. Aging enhances the basal production of IL-6 and CCL2 in vascular smooth muscle cells. *Arterioscler Thromb Vasc Biol.* 2012;32:103–109. DOI: 10.1161/ATVBAHA.111.236349.

32. Gardner SE, Humphry M, Bennett MR, Clarke MC. Senescent vascular smooth muscle cells drive inflammation through an interleukin-1α-dependent senescence-associated secretory phenotype. *Arterioscler Thromb Vasc Biol.* 2015;35:1963–1974. DOI: 10.1161/ATVBAHA.115.305896.

33. Wang J, Uryga AK, Reinhold J, Figg N, Baker L, Finigan A, Gray K, Kumar S, Clarke M, Bennett M. Vascular smooth muscle cell senescence promotes atherosclerosis and features of plaque vulnerability. *Circulation.* 2015;132:1909–1919. DOI: 10.1161/CIRCULATIONAHA.115.016457.

34. Sano N, Satow T, Maruyama D, Kataoka H, Morita K, Ishibashi-Ueda H, Iihara K. Relationship between histologic features and outcomes of carotid revascularization for radiation-induced stenosis. *J Vasc Surg.* 2015;62:370–377.e371. DOI: 10.1016/j.jvs.2015.03.021.

35. Wang Y, Schulte BA, LaRue AC, Ogawa M, Zhou D. Total body irradiation selectively induces murine hematopoietic stem cell senescence. *Blood.* 2006;107:358–366. DOI: 10.1182/blood-2005-04-1418.

36. Xie M, Lu C, Wang J, McLellan MD, Johnson KJ, Wendl MC, McMichael JF, Schmidt HK, Yellapantula V, Miller CA, et al. Age-related mutations associated with clonal hematopoietic expansion and malignancies. *Nat Med.* 2014;20:1472–1478. DOI: 10.1038/nm.3733.

37. Libby P, Ebert BL. CHIP (clonal hematopoiesis of indeterminate potential): potent and newly recognized contributor to cardiovascular risk. *Circulation.* 2018;138:666–668. DOI: 10.1161/CIRCULATIONAHA.118.034392.

38. Jaiswal S, Natarajan P, Silver AJ, Gibson CJ, Bick AG, Shvartz E, McConkey M, Gupta N, Gabriel S, Ardissino D, et al. Clonal hematopoiesis and risk of atherosclerotic cardiovascular disease. *N Engl J Med.* 2017;377:111–121. DOI: 10.1056/NEJMoa1701719.